Effect of attapulgite calcination on heavy metal adsorption from acid mine drainage

Thabo Falayi and Freeman Ntuli[†]

Department of Chemical Engineering, University of Johannesburg, P. O. Box 17011,
Doornfontein 2028, Johannesburg, South Africa

Abstract−Attapulgite calcined at 973.15K was characterized and utilized as an adsorbent for the removal of heavy metals and neutralization of acid mine drainage (AMD) from a gold mine. Batch adsorption experiments were carried out using a thermostatic shaker. Activated attapulgite showed that it can neutralize AMD as it raised the pH from 2.6 to 7.3 after a residence time of 2 h. Metal ion removal after 2 h was 100% for Cu (II), 99.46% for Fe (II), 96.20% for Co (II), 86.92% for Ni (II) and 71.52% for Mn (II) using a 2.5% w/v activated attapulgite loading. The adsorption best fit the Langmuir isotherm; however, Cu (II), Co (II), and Fe (II) data fit the Freundlich isotherm as well. Calcination at 973.15 K resulted in the reduction of the equilibrium residence time from 4 to 2 h, solid loading reduction from 10 to 2.5% m/v and an increase in maximum adsorption capacity compared with unactivated attapulgite.

Keywords: Acid Mine Drainage, Attapulgite, Calcination, Adsorption, Heavy Metal Removal

INTRODUCTION

Acid mine drainage (AMD) is polluted water that results when sulfur bearing minerals associated with coal and gold mining are exposed to air and water, resulting in the formation of sulfuric acid and ferrous sulfate [1]. When pyrite is exposed to water and oxygen, oxidation and hydrolysis reactions produce sulfur acid (H_2SO_4) and free hydrogen ions (H^+), acidifying the water. The acidic medium allows other metals which are associated with the ore, such as Cd, Fe, Cu, Pb, Ni, Mn and Zn, to be dissolved into solution [2]. At pH levels above 4.0 the ferrous iron spontaneously oxidizes to ferric iron, which in turn reacts with water to release three hydrogen ions for every ferric ion reacted, driving the pH further down. When the pH is below 3.0, iron-oxidizing bacteria such as Thiobacillus ferrooxidans thrive, rapidly converting ferrous iron to ferric iron, producing additional acidity. Acid mine drainage in South Africa, in particular in the western and central basins of Witwatersrand catchment area, is now perceived as a national crisis [3]. AMD has been shown to contaminate surface and ground water, damaging the health of plants, wild life and fish [4]. In England and Wales, it is estimated that some 1,800 km of surface streams and rivers are currently impacted by AMD, whereas in Spain, 427 km of river network is affected by AMD [5]. Heavy metals (one of the constituents of AMD) present serious environmental challenges since they are not biodegradable and can be retained in organic tissues through bioaccumulation leading to biomagnification at higher trophic levels [6]. A variety of treatment methods have been developed for heavy metal removal, including precipitation, adsorption, ion-exchange and membrane technologies. Adsorption using clays has been shown to be a useful, cost effective method for heavy metal removal from AMD [7,8]. Unactivated attapulgite at 10%

(m/v) solid loading has been shown to remove at least 93% of Co, Cu, Ni and Fe whilst removing 66% Mn [9]. To reduce the solid loading of the adsorbent there was a need to activate the attapulgite. Activation reduces the solid loading, which leads to an increase in mass transfer and reduces the challenges encountered with abrasion of process equipment and pumping of clay slurries. This research seeks to establish the effect of attapulgite calcination as an activation method to enhance adsorption. AMD was obtained from a local gold mine and was fortified to fully reflect the average AMD composition in the Gauteng province of South Africa [3,10].

MATERIALS AND METHODS

Thermally activated attapulgite was used in the sorption experiments. The effect of adsorbent loading, agitation time and temperature on the removal of heavy metals and neutralization of AMD was investigated. Adsorption isotherms, kinetics and thermodynamic parameters were calculated from the data obtained. Desorption studies were carried out to recover metal ions from metal loaded activated attapulgite to provide for possible re-use of metal loaded activated attapulgite.

1. Materials

Acid mine drainage was collected from a local gold mine and analyzed to find the concentration of heavy metals and other elements present. Attapulgite was supplied by G&W Base Minerals. Analytical grades of $FeSO_4 \cdot 7H_2O$, $CoSO_4 \cdot 7H_2O$, $CuSO_4 \cdot 5H_2O$ and $NiSO_4 \cdot 6H_2O$ were supplied by Sigma Aldrich.

2. Apparatus

The pH and conductivity were measured using Mettler Toledo dual meter (Sevenduo pH/conductivity meter with a Mettler Toledo InLab Pro ISM pH electrode and Mettler Toledo InLab738 ISM conductivity probe). Metal analysis was achieved using an atomic absorption spectrometer (Thermo scientific ICE 3000 Series). An XRF (Rigaku ZSX Primus II) was used to analyze for elemental composition of attapulgite. Fourier transform infrared spectros-

[†]To whom correspondence should be addressed.
E-mail: fntuli@uj.ac.za

Table 1. AMD parameters

Parameter	Before fortification	After fortification
pH	2.66	2.84
Temperature (°C)	23.4	23.3
Conductivity (mS/cm)	2.62	5.77
Sulphates (ppm)	2820	3520
Fe (ppm)	4	532
Mn (ppm)	120	114
Ni (ppm)	Below detection limit	20.4
Cu (ppm)	Below detection limit	15.7
Co (ppm)	Below detection limit	21.3

copy (Thermoscientific Nicket IS10) was used to characterize attapulgite before and after the adsorption experiments. Adsorption experiments were conducted in a thermostatic shaker (Labotec OrbiShaker). A UV Visible spectrophotometer (PG Instruments T60) was used to measure sulfate content. The mineralogical composition of the attapulgite was determined using an XRD (Ultima IV Rigaku XRD). Particle size distribution was measured by a laser diffraction technique using a Malvern Mastersizer 2000 instrument.

3. Fortification of Acid Mine Drain

To 100 ml of AMD were added appropriate amounts of sulfate salts of Fe, Co, Cu and Ni. The solution was stirred at 200 rpm for 10 min and made up to 1,000 ml with raw AMD while stirring for a further 20 min. Table 1 shows the AMD parameters before and after fortification.

4. Activation of Attapulgite

Attapulgite was activated thermally at 473.15, 673.15 and 973.15 K in an oxidizing furnace for 4 h.

5. Batch Adsorption

5-1. Effect of Adsorbent

2-4 g of the 973.15 K calcined attapulgite (here after referred to as activated attapulgite) and 10 g attapulgite calcined at 473.15 and 673.15 K (labelled 10A and 10B, respectively) were added to different 100 ml solutions of fortified AMD. The solutions were agitated at 200 rpm using a thermostatic shaker maintained at 298.15 K for 2 h. After 2 h, agitation was stopped and the solution pH and conductivity were measured. The solutions were then subsequently filtered using a Buchner funnel and acidified with 1 drop of concentrated nitric acid and stored at 277.15 K awaiting metal analysis using AAS. Sulfate content was measured with a UV-VIS spectrophotometer by using the Environmental Protection Agency (EPA) method 3754.

5-2. Effect of Initial Concentration

The initial metal concentration of Fe, Cu, Co and Ni was increased as shown in Table 4. 100 ml of the resulting AMD solutions was then added to 2.5 g of activated attapulgite. The solutions were agitated at 200 rpm with a thermostatic shaker maintained at 298.15 K for 2 h. The solutions were then subsequently filtered by Buchner funnel and acidified with 1 drop of concentrated nitric acid and stored at 277.15 K awaiting metal analysis by using AAS.

5-3. Effect of Residence Time and Temperature

2.5 g of activated attapulgite was added to 100 ml of fortified AMD, in a 250 ml conical flask. The initial pH and conductivity,

of the fortified AMD were measured. Four solutions were used and each solution was agitated at 200 rpm using a thermostatic shaker maintained at 298.15 K. The solutions were run for 0.5, 1, 1.5 and 2 h, respectively. After each time interval, agitation was stopped and the solution pH and conductivity were measured. The solutions were then subsequently filtered using a Buchner funnel and acidified with 1 drop of concentrated nitric acid and stored at 277.15 K awaiting metal analysis by AAS. The amount of metal adsorbed per unit mass of adsorbent at equilibrium q_e is given by:

$$q_e = (C_0 - C_e) \times V/M \tag{1}$$

where C_o (ppm) is the initial metal concentration in the AMD, C_e is the metal concentration at equilibrium, V (L) is the volume of the AMD and M (g) is the mass of the adsorbent. The above procedure was then repeated at 308.15 K and 318.15 K to calculate thermodynamic parameters.

5-4. Reuse of Metal Loaded Activated Attapulgite

Metal-loaded activated attapulgite was dried in an oven at 323.15 K for 12 h. After drying, the metal loaded activated attapulgite was crushed to a fine powder using a mortar and pestle. 2.5 g of metal loaded activated attapulgite was then added to fresh fortified AMD and was agitated at 200 rpm using a thermostatic shaker maintained at 298.15 K. After agitation the solution pH and conductivity were measured. The solution was then subsequently filtered using a Buchner funnel and acidified with 1 drop of concentrated nitric acid and stored at 277.15 K awaiting metal analysis using AAS. This metal loaded activated attapulgite was re-used once following the outlined procedure. In total the attapulgite was used in two separate treatment cycles.

5-5. Desorption Studies

To explore the possibility of recycling activated attapulgite, desorption studies were conducted. 2.5 g of metal loaded activated attapulgite was added to 100 ml of 0.05 M HNO₃ (pH 2.0) and agitated at 200 rpm using a thermostatic shaker maintained at 298.15 K. After 2 h, the solution was then subsequently filtered using a Buchner funnel and acidified with 1 drop of concentrated nitric acid and stored at 277.15 K awaiting metal analysis using AAS.

6. Theory and Statistics

6-1. Adsorption Isotherms

To study the thermodynamic behavior of the adsorption process, adsorption isotherms were used. To find the adsorption capacities of activated attapulgite for different metal ions, the experimental results were analyzed by using the Langmuir (Eq. (2)) and Freundlich (Eq. (3)) isotherms. The following linearized equations were used for this purpose:

$$C_e/q_e = 1/q_m \cdot b + C_e/q_m \tag{2}$$

$$\log q_e = \log K_F + 1/n \log C_e \tag{3}$$

where C_e (mg/L) is the metal concentration in solution at equilibrium, q_e (mg/g) is the amount of metal adsorbed per unit mass of adsorbent, q_m (mg/g) is the maximum adsorption capacity, b (L/g) is a constant related to enthalpy of adsorption, K_F and n are Freundlich equilibrium constants indicative of the adsorption capacity and adsorption intensity.

The Langmuir isotherm can be characterized by a dimension-

less constant R_L, called equilibrium constant:

$$R_L = 1/1 + bC_0 \tag{4}$$

6-2. Adsorption Kinetics

To study adsorption kinetics the experimental data was fitted into the pseudo-first-order plot (Eq. (5)), pseudo-second-order plot (Eq. (6)), Elovich equation plot (Eq. (7)), Webber Morris intraparticle plot (Eq. (8)) and Liquid film diffusion model plot (Eq. (9)) represented by Eqs. (5)-(9), respectively.

$$\log(q_e - q_t) = \log q_e - (k_1/2.303)t \tag{5}$$

where q_t (mg/g) is the amount adsorbed at any time per unit mass of adsorbent, k_1 is the rate constant (min^{-1}). A plot of $\log(q_e - q_t)$ vs t should be linear if the model fits the experimental data.

$$t/q_t = 1/k_2 q_e^2 + (1/q_e)t \tag{6}$$

A plot of t/q_t vs t should be linear if the model fits the experimental data.

$$q_t = (1/\beta)\ln(\alpha\beta) + (1/\beta)\ln t \tag{7}$$

where α and β are Elovich constants representing initial adsorption rate and the desorption rates. A plot of q_t vs ln t should be linear if the model fits the experimental data.

$$q_t = k_1 t^{0.5} \tag{8}$$

A plot of q_t vs $t^{0.5}$ should be linear with 0 as the intercept if the model fits the experimental data.

$$\ln(1-F) = -k_{fd}t \tag{9}$$

$$F = q_t/q_e \tag{10}$$

A plot of $-\ln(1-F)$ vs t should be linear with a zero intercept if the model fits the experimental data.

6-3. Adsorption Thermodynamics

The Langmuir constant, b, can be used to estimate the enthalpy, entropy and Gibbs energy changes accompanying adsorption, based on Eqs. (11)-(16).

$$\Delta G^0 = -RT \ln b \tag{11}$$

where ΔG^0 is the standard free energy change, J/mol, R is the universal gas constant, 8.314 J/mol K; and T is absolute temperature, K. Considering the relationship between ΔG^0 and b the change in equilibrium constant with temperature can be obtained in a differential form as follows:

$$d \ln b/dT = \Delta H^0/RT^2 \tag{12}$$

After integration the equation becomes

$$\ln b = -(\Delta H^0/RT) + Y \tag{13}$$

$$RT \ln b = TRY - \Delta H^0 \tag{14}$$

$$\Delta S^0 = RY \tag{15}$$

Using Eq. (11)

$$\Delta G^0 = \Delta H^0 - T\Delta S^0 \tag{16}$$

A plot of ΔG^0 versus temperature, T, will be linear and the values of ΔH^0 and ΔS^0 can be determined from the intercept and slope of the plot, respectively.

6-4. Statistics

All metal analysis was done in duplicate with the final results being the arithmetic average of results that were between 5% of each other. All isotherm, kinetic and Gibbs free energy graphs were drawn using the linear least squares regression method. To determine the applicability of models the value of the correlation coefficient (r) was used. The value of r was computed using Eq. (17):

$$r(x,y) = \sum(x-\bar{x})(y-\bar{y})/\sqrt{\sum(x-\bar{x})^2(y-\bar{y})^2} \tag{17}$$

where x, y represent variables and $\bar{x}$ and $\bar{y}$ are the average (arithmetic mean) of the variables.

RESULTS AND DISCUSSION

1. Characterization of Activated Attapulgite and Metal Loaded Activated Attapulgite

Table 2 shows the chemical composition of unactivated attapulgite, activated attapulgite and metal loaded activated attapulgite.

Table 2. XRF analysis of attapulgite

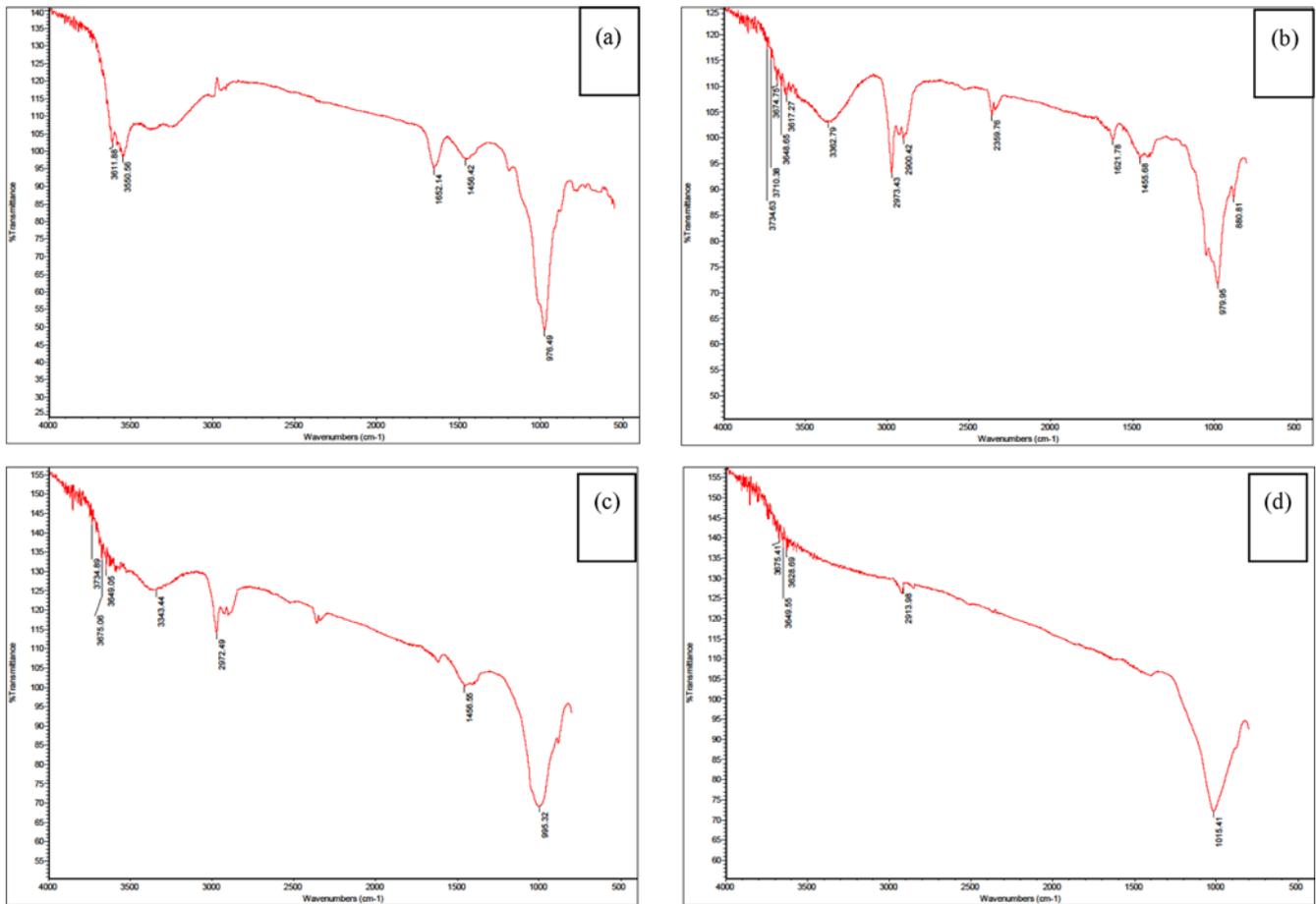| Oxide (%m/m)	Unactivated attapulgite	Attapulgite calcined @ 473.15 K	Attapulgite calcined @ 673.15 K	Attapulgite calcined @ 973.15 K	Metal loaded activated attapulgite
Na_2O	0.136	0.136	0.128	0.162	0.198
MgO	11.4	11.4	12.0	12.5	11.2
Al_2O_3	9.91	9.91	10.1	9.90	10.2
SiO_2	68.4	65.7	66.3	65.6	65.1
SO_3	0.171	0.171	0.205	0.202	0.613
K_2O	0.585	0.554	0.592	0.589	0.552
CaO	4.19	4.27	4.30	4.54	2.52
TiO_2	0.484	0.566	0.568	0.576	0.547
MnO	0.0640	0.076	0.0700	0.0805	0.353
Fe_2O_3	4.09	4.10	5.15	5.29	8.06
Co_2O_3	0.00280	0.00540	0.00280	0.00280	0.0764
NiO	0.0115	0.112	0.152	0.0151	0.0672
CuO	0.00330	0.00440	0.00610	0.00660	0.124

Fig. 1. FTIR spectra for unactivated attapulgite (a) and attapulgite calcined at 473.15 K (b) at 673.15 K (c) and 973.15 K (d).

Silica was the major constituent. Calcination of attapulgite results in a slight decrease in silica content at all temperatures used. There was an increase in the relative content of Fe_2O_3, MgO and CaO content at 673 and 973 K. Overall, the proportion of neutralizing bases (MgO and CaO) increased with increasing calcination temperature (Table 2).

1-2. Effect of Calcination on the Structure of Attapulgite

Fig. 1 shows different FTIR spectra of attapulgite calcined at different temperatures.

An asymmetric band centered at 1,621 and 1,455 cm^{-1} in the sample corresponds to the bending vibration modes of water molecules and can be resolved as bands which are attributed to the bound water and adsorbed water, respectively [11]. Bound water is driven off at 673.15 K and adsorbed water is driven off at 973.15 K (Fig. 1). There is also a gradual decrease in the intensity of the band at 3,200-3,800 cm^{-1} which is associated with OH stretching of water coordinated to Al, Mg and zeolitic water [12], although the band intensity slightly increased at 473.15 K because of the re-adsorption of water during the experimental procedure as has been reported by other researchers [13].

1-3. Effect of Calcination on Mineral Composition of Attapulgite

Fig. 2 shows the XRD spectra of attapulgite heated at different temperatures.

Heating to 673.15 K did not result in substantial collapse in the

palygorskite peak at 2θ of 8.26°. The relative intensity of the peak decreased from 61.17 (unactivated attapulgite) to 57.52 (attapulgite calcined at 673.15 K). Calcination at 973.15 results in substantial collapse of the palygorskite structure with its peak relative intensity decreasing to 7.94. Similar results have been reported [14-16]. The intensity of the dolomite peak was not affected by calcination up to 673.15 K but decreased significantly at 973.15 K.

1-4. Effect of Calcination on Specific Surface Area, External Surface Area and Particle Size Distribution of Attapulgite

Table 3 shows the variation of specific surface, external surface area, pore volume and pore size with calcination temperature. The external surface area was calculated from the PSD generated by laser diffraction by first transforming the volume distribution to a number density distribution and then using the method of moments to calculate the second moment (m_2 equivalent to external surface area) [17]. Fig. 3 shows the number density distribution for activated and unactivated attapulgite.

There was a decrease in specific surface area and a small increase in pore volume and pore size of attapulgite as the temperature of calcination was increased in agreement with previous research work [18]. This can be explained by the collapse of the palygorskite structure as temperature is increased as confirmed by XRD results [16]. External surface area increased with increases in calcination temperature, which can be explained by the corresponding increase in
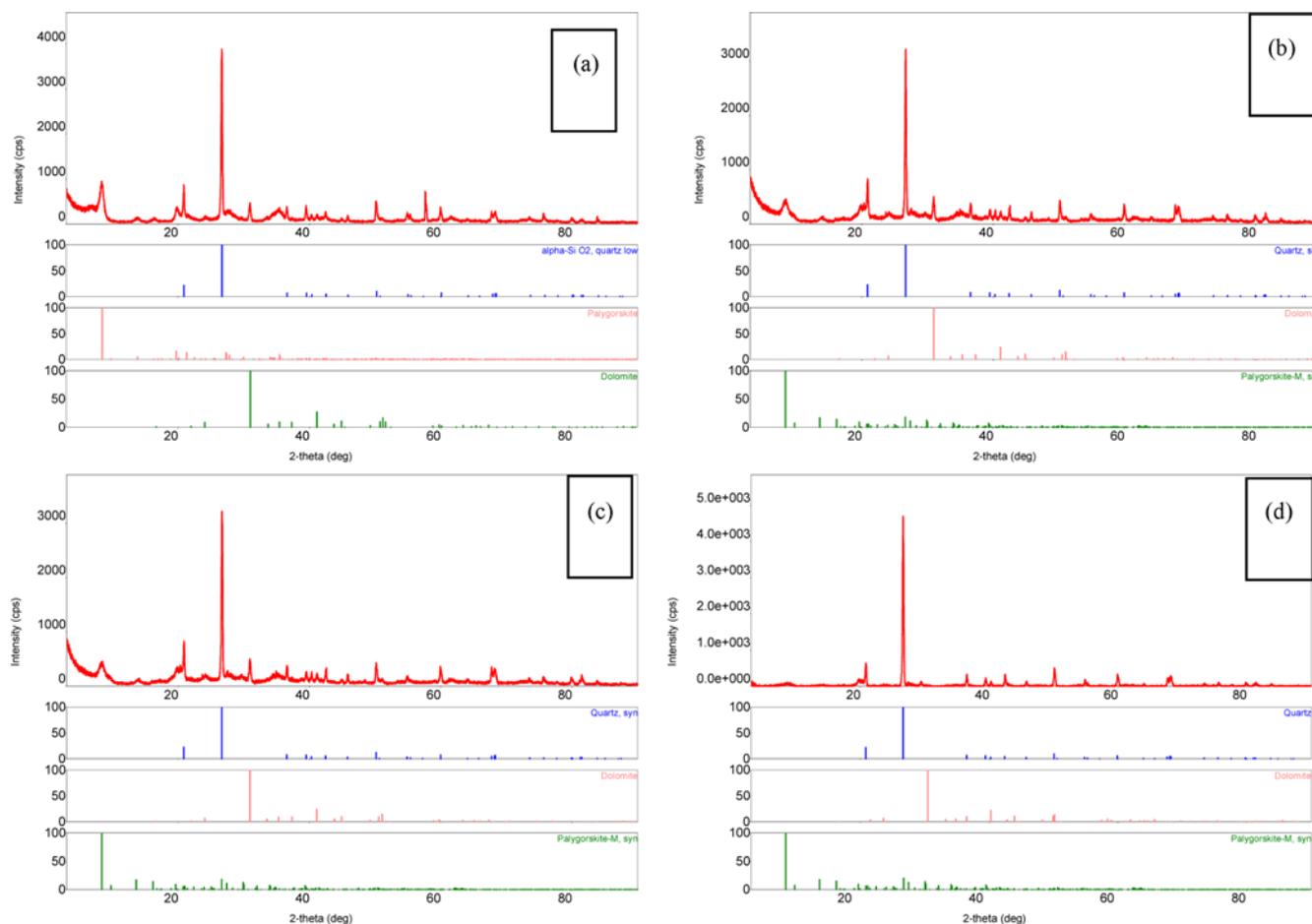
Fig. 2. XRD spectra for unactivated attapulgite (a) and attapulgite calcined at 473.15 K (b), 673.15 K (c) and 973.15 K (d).

Table 3. Variation in attapulgite physical properties with temperature

Attapulgite	Surface area (cm²/g)	Pore volume (cm³/g)	Pore size (Å)	External surface area ($\times 10^3$ m²m⁻³)
Uncalcined attapulgite	127	0.330	103	2.78
Calcined at 473.15 K	106	0.254	96.1	2.99
Calcined at 673.15 K	102	0.268	105	3.58
Calcined at 973.15 K	85.9	0.284	129	5.81

number of particles under 2.8 μm for attapulgite calcined at 973.15 K (Fig. 3). The collapse of the palygorskite structure at high calcination temperature results in palygorskite fibers shrinking, leading to the space between the layers being reduced hence the increase in the number of small sized particles [18].

2. Effect of Adsorbent Dosage

Fig. 4 shows the variation in pH and conductivity with adsorbent mass. 1-4% solid loading refers to the solid loading used for experiments conducted with activated attapulgite; whereas 10A and 10B refer to attapulgite calcined at 473.15 and 673.15 K, respectively, and used at a solid loading of 10%. 2.5% m/v loading of activated attapulgite could neutralize AMD to a pH of 7.3 after 2 h with a reduction in conductivity to 3.42 mS/cm (Fig. 4). 10% m/v loading of 10A and 10B could only achieve a pH of around 6.3. The increase in pH is due to the increase in the neutralizing cations (CaO and Na₂O) as the quantity of activated attapulgite is increased.

The reduction in conductivity can be attributed to heavy metal removal as seen in Fig. 5.

Fig. 5 shows the variation of metal removal with adsorbent loading using 2-4% m/v activated attapulgite and 10% m/v 10A and 10B loading.

10% (m/v) loading of attapulgite calcined at 473.15 K and 673.15 K was effective in removal of Fe and Cu only (Fig. 5) but was not effective for other metal ions. There was an increase in metal removal as the adsorbent dosage was increased from 2% to 4% for attapulgite calcined at 973.15 K. The increase in percent removal with adsorbent mass (up to 4% loading) can be attributed to an increase in adsorption sites with increasing mass of adsorbent. To eliminate removal of metals exclusively by precipitation the 2.5% (m/v) loading was chosen for subsequent experiments as the solubilities of the various metal hydroxides are minimized in the pH range of 8.0-11.0 resulting in precipitation.
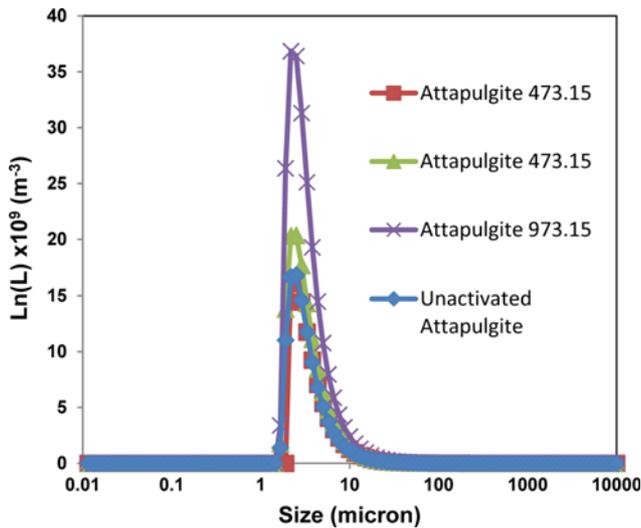
Fig. 3. Number density distribution for activated and unactivated attapulgite.
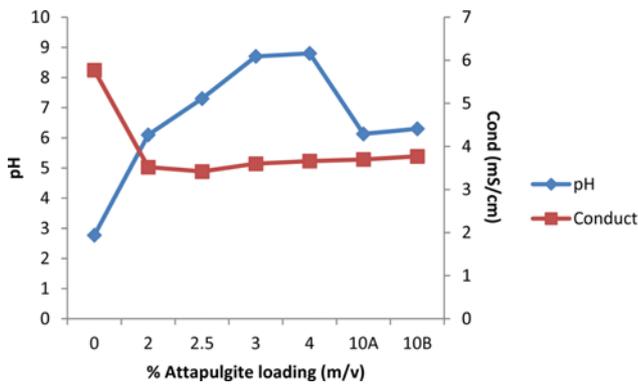

Fig. 4. Variation of pH and conductivity with adsorbent mass (0% loading represents the initial pH and conductivity values).
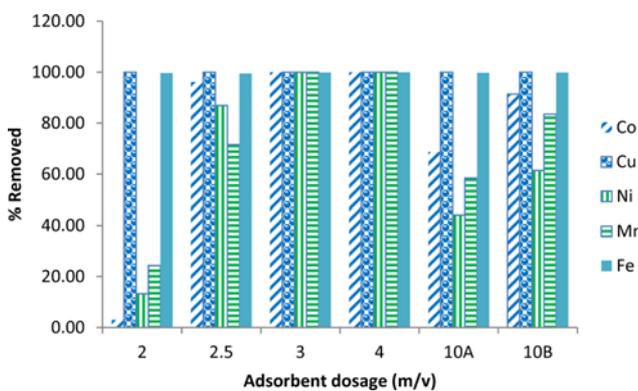

Fig. 5. Variation in metal removal with adsorbent loading (initial concentrations given in Table 5 solution 1).

After 2 hours of agitation using 2.5% m/v solid loading of atta-pulgite calcined at 973.15 K the concentration of sulfates was reduced from 3,600 ppm to 3,352 ppm representing a 6.9% reduction in sul-fate concentration. Therefore, activated attapulgite was not effec-tive in adsorbing sulfates from AMD.

Table 4. Variation in % removal with initial concentration

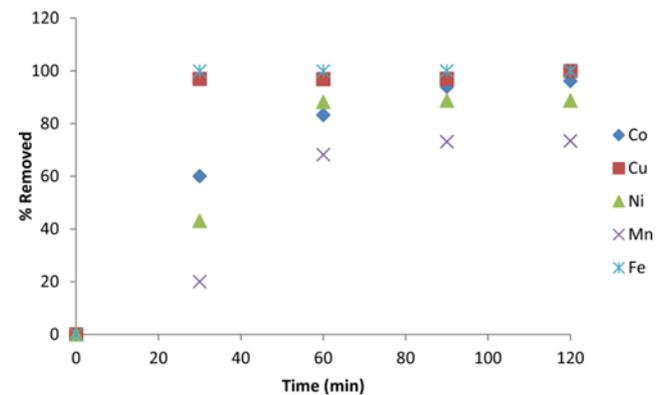|	Solution 1	
Metal	Concentration (ppm)	% Removal
Fe	507	99.6
Ni	16.8	86.9
Cu	20.0	100
Co	19.9	96.2
	Solution 2	
Fe	998	99.3
Ni	34.3	60.0
Cu	40.0	100
Co	39.0	58.3
	Solution 3	
Fe	1600	74.8
Ni	50.3	29.3
Cu	59.7	97.3
Co	61.2	23.3

Fig. 6. Variation in metal adsorbed with time (initial concentrations given in Table 4, solution 1).

3. Effect of Initial Concentration

Table 4 shows the variation in % metal removal with initial con-centration using 2.5% m/v solid loading of attapulgite calcined at 973.15 K. Table 4 shows that there was no significant decrease in % Cu removed as the initial concentration was increased. For other metals there was a decrease in metal removal with an increase in concentration. This is due to increase in competition for adsorp-tion sites at higher metal concentration [19]. Cu is not affected as it has the least K_{sp} and pK_h values as compared to other heavy metal cations in solution, meaning that Cu has less affinity for solvent and greater affinity for the adsorbent [20].

4. Adsorption Isotherms

Fig. 6 shows the variation of metal adsorbed per unit mass of activated attapulgite with time using 2.5% m/v solid loading of atta-pulgite calcined at 973.15 K. Equilibrium was reached within 20 min for Cu and Fe; however, for the other metals equilibrium was reached after 60 min. The results showed that metal ion removal after 2 h was 100% for Cu, 99.46% for Fe, 96.20% for Co, 86.92% for Ni and 71.52% for Mn using a 2.5% w/v activated attapulgite loading. To obtain more accurate thermodynamic and kinetic data for Fe and
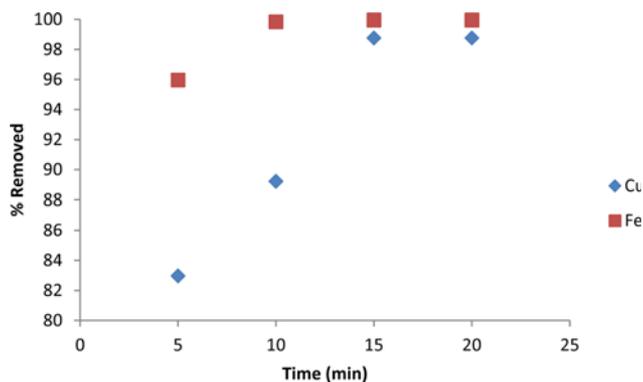
Fig. 7. Variation in metal adsorbed with time for Fe and Cu (initial concentrations given in Table 4, solution 1).

Cu, data sampling was done at 5 min interval up to 20 min as shown in Fig. 7.

Table 5 shows the Langmuir and Freundlich parameters using 2.5% m/v solid loading of attapulgite calcined at 973.15 K.

Co, Mn, Ni, Cu and Fe experimental data fitted well the Langmuir isotherm as $R^2 \geq 0.999$ (Table 5). Since $0 < R_L < 1$ (Table 5), for Cu, Co, Ni, Mn and Fe, it shows that the adsorption was thermodynamically favorable [21]. Co, Cu and Fe experimental data fit-

ted the Freundlich isotherm well as $R^2 \geq 0.999$ (Table 5). n values between 1 and 10 for the Freundlich isotherm indicate thermodynamically favorable adsorption [22], since the value of n in the Freundlich isotherm for Cu and Fe is greater than 10, (Table 5) adsorption of Cu and Fe is not thermodynamically favorable but the adsorption of Co is thermodynamically favorable.

5. Adsorption Kinetics

Table 6 shows the kinetic parameters for the pseudo-first and second-order kinetics, Elovich model, intraparticle diffusion model and liquid diffusion model using 2.5% m/v solid loading of attapulgite calcined at 973.15 K.

Ni and Mn experimental data fit the pseudo-first-order kinetics as R^2 values ≥ 0.99 (Table 6) whilst Co, Cu and Fe experimental data fit the second-order kinetics as $R^2 \geq 0.99$ (Table 6). The Elovich model did not give a satisfactory fit to the experimental data as R^2 values were below 0.99 for all metals (Table 6). Thus, it was concluded that the adsorption process was not via chemisorption [23], which is also supported by thermodynamic calculations which showed that the Gibbs free energy values were less than -20 kJ/mole, thus indicating physisorption [24]. The intraparticle diffusion model did not fit as $R^2 \leq 0.9$ for all metals (Table 6); thus, intraparticle diffusion was not the rate-limiting step. Liquid diffusion model plots were linear for Mn and Ni as $R^2 \geq 0.99$, but the intercepts were not zero, hence, liquid diffusion was not the rate limiting step. Fe, Cu

Table 5. Langmuir and Freundlich parameters

Metal	Langmuir parameters				Freundlich parameters		
	Q_{max} (mg/g)	b (Lg^{-1})	R^2	R_L	K_F	n	R^2
Co	0.0101	0.766	0.9998	0.0594	0.0260	2.70	0.999
Cu	0.0188	51.5	1.0000	0.000928	0.0190	31.9	1.000
Ni	0.00800	1.14	0.9967	0.0421	0.0260	2.90	0.950
Mn	0.00290	0.0420	0.9957	0.184	0.869	0.800	0.989
Fe	0.0200	13200	1.0000	0.000000100	0.0200	2500	0.999

Table 6. Kinetic parameters

Metals	Ni	Co	Cu	Mn	Fe
Pseudo first order parameter					
q_e (mg/g)	0.116	0.0277	0.0000500	0.152	5.00E-06
K_1 (min^{-1})	0.0790	2.17	0.930	0.0850	0.0230
R^2	0.995	0.943	0.404	0.996	0.807
Pseudo second order parameters					
q_e (mg/g)	0.0298	0.0193	0.0194	0.0792	0.0200
K_2	3.54	0.570	1070	0.0300	8540
R^2	0.868	0.990	1.00	0.0850	1.000
Elovich model parameters					
R^2	0.842	0.815	0.250	0.842	0.845
Intra particle diffusion parameters					
Intercept	0.000	0.00800	0.00200	0.00400	0.00200
R^2	0.770	0.734	0.319	0.764	0.898
Liquid difusion parameters					
Intercept	1.82	0.491	6.32	2.34	8.28
R^2	0.997	0.943	0.404	0.996	0.807

Table 7. Langmuir isotherms parameters at different temperatures

T (K)	Q_{max} (mg/g)	b (L/g)	R^2	R_L	ΔG^o (J/mol)
Co					
298.15	0.0101	0.766	0.9998	0.0594	661
308.15	0.0121	1.50	0.9934	0.800	−1040
318.15	0.0138	2.83	0.9950	0.0168	−2750
Ni					
298.15	0.00800	1.14	0.9967	0.0421	−322
308.15	0.0106	1.11	0.9980	0.825	−272
318.15	0.0109	1.07	0.9985	0.822	−179
Cu					
298.15	0.0188	51.5	1.000	0.000900	−9770
308.15	0.0127	106	1.000	0.790	−11900
318.15	0.0200	496	1.000	0.705	−16400
Mn					
298.15	0.00290	0.0417	0.9957	0.184	7880
308.15	0.00860	0.142	0.9700	0.522	5010
318.15	0.00359	0.337	0.9750	0.724	2880
Fe					
298.15	0.0200	13200	1.000	1.48E-07	−23500
308.15	0.0143	11700	1.000	0.120	−24000
318.15	0.0200	12500	1.000	0.0891	−25000

Fig. 8. Gibbs free energy plots for Co, Cu, Ni, Fe and Mn.

Table 8. Variation in metal removal

Metal	% Removal
Cu	2.55
Co	86.1
Ni	2.65
Mn	1.25
Fe	73.3

and Co plots were not linear as $R^2 \leq 0.99$, hence liquid diffusion was not the rate-limiting step as the solution was adequately agitated at 200 rpm. Thus, it can be concluded that the interaction between the adsorbent and the adsorbate was the rate-limiting step.

6. Thermodynamics

Fig. 7 shows the Gibbs free energy plots and Table 7 shows the variation of Langmuir isotherm parameters with temperature.

There was a decrease in the negative value of ΔG^0 for Cu and Fe with increase in temperature (Table 7). The decrease in the negative value of ΔG^0 with an increase in temperature indicated that the adsorption process of these ions onto activated attapulgite becomes more favorable at higher temperatures. The negative ΔG^0 values mean the process is thermodynamically spontaneous. ΔG^0 value for Co became negative as temperature was increased, showing that the adsorption process of Co onto activated attapulgite becomes more favorable at higher temperatures. There was an increase in negative value of ΔG^0 for Ni. The increase in negative value means that adsorption of Ni on activated attapulgite becomes less spontaneous at higher temperatures. ΔG^0 values up to −20 kJ/mol are consistent with electrostatic interaction between adsorption sites and the metal ion, physisorption [24]. There was a decrease in the positive value of ΔG^0 for Mn with an increase in temperature. The positive value of ΔG^0 shows that the sorption process is not thermodynamically feasible. The values of ΔH^0 for Cu, Co and Mn were 89.71 kJ/mol, 51.59 kJ/mol and 82.34 kJ/mol, respectively, indicating that the adsorption process was endothermic. The values of ΔH^0 for Ni and Fe were −2.47 kJ/mol and −1.93 kJ/mol indicating that the adsorption process was exothermic. The values of ΔS^0 for Co, Cu, Mn and Fe were 170.8 J/mol, 332 J/mol, 250.1 J/mol and 72.13 J/mol, respectively, indicating the affinity of the acti-

vated attapulgite for the metals ions and some structural changes at the adsorbate and adsorbent interface [25]. The value for ΔS^0 for Ni −7.17 J/mol indicates a decrease in randomness at the solid/solution interface [26]. Fig. 8 shows the FTIR spectra for activated attapulgite and metal loaded activated attapulgite.
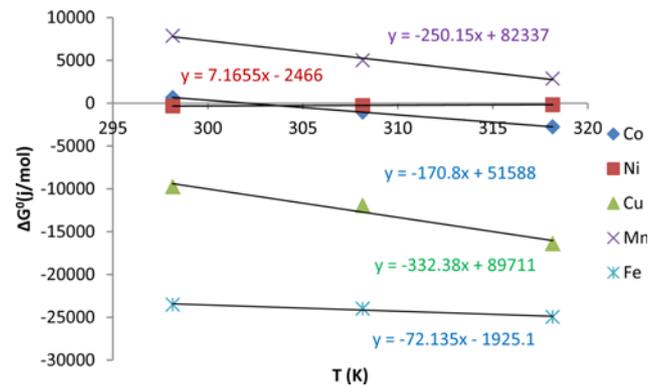
The precipitation of hydroxides was not confirmed by measuring the FTIR spectra as Cu-OH, Mn-OH, Ni-OH and Fe-OH bands at 1,382 cm^{-1}, 1,550-1,850 cm^{-1}, 600 cm^{-1} and 3,360 cm^{-1}, respectively, were not present in the metal-loaded activated attapulgite spectrum [27-30].

CaO decreased by 2.02% after adsorption, meaning Ca is the dominant exchangeable ion. An increase in MnO, Fe_2O_3, Co_2O_3, NiO and CuO content in the metal loaded activated attapulgite was a result of ion exchange (Table 2).

7. Re-use of Adsorbent

Table 8 shows the variation in metal removal using metal loaded activated attapulgite.

Metal-loaded activated attapulgite was not effective in Cu, Ni and Mn removal once it had been used as only 2.55% of Cu was adsorbed. However, it was effective in the removal of Fe and Co (Table 8); thus it is essential to regenerate the adsorbent before reuse.

8. Desorption Studies

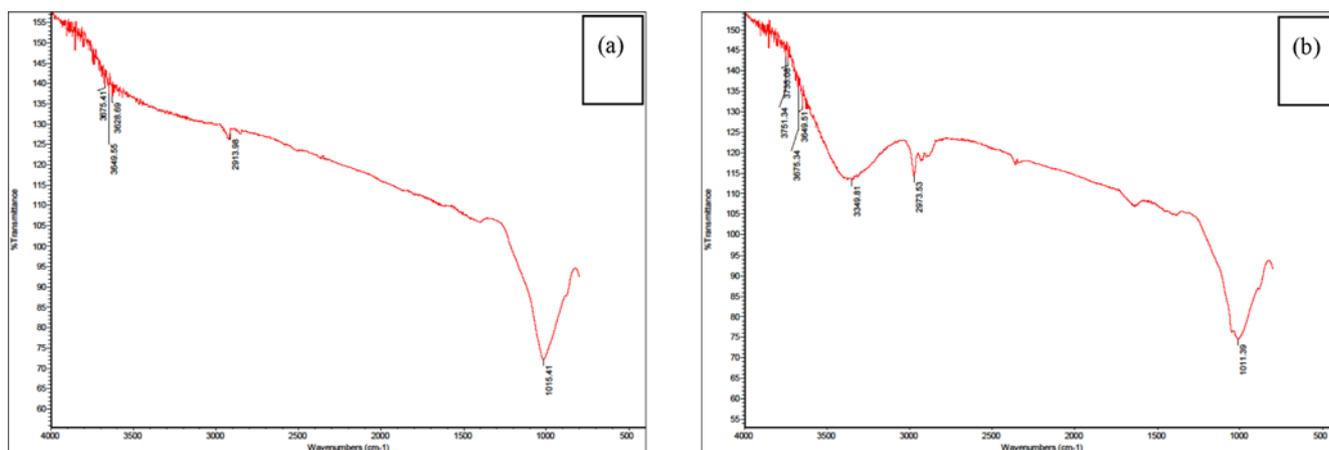Table 9 shows the percentage metal recovered from metal-loaded activated attapulgite.

From Table 9 it can be concluded that 0.05 M HNO_3 can be used to recover most of the metals with the exception of Fe where removal was below 50%. ΔG^0 for the adsorption for Fe was the highest at −23.5 kJ/mole, meaning that Fe desorption is not spontaneous.

9. Comparison between Unactivated Attapulgite and Activated Attapulgite

A comparison between unactivated [9] and activated attapulgite is detailed as follows. Unactivated attapulgite requires 10% m/v

Table 9. Metal concentrations removed from metal loaded activated attapulgite

	Original concentration (ppm)	Concentration after agitation (ppm)	Concentration metal loaded activated attapulgite (ppm)	Adsorbed from AMD (ppm)	% Leached from metal loaded activated attapulgite (ppm)
Fe	0	230	230	532	43.2
Mn	0	45.3	45.3	71.9	63.0
Co	0.130	16.3	16.2	18.9	85.7
Ni	0.284	13.5	13.3	16.3	81.6
Cu	0.0380	12.3	12.2	15.4	79.2

Fig. 9. FTIR spectra for Activated attapilgite (a) and metal loaded attapulgie (b).

loading while activated attapulgite requires 2.5% m/v loading. This is because activated attapulgite has more small particles as compared to unactivated attapulgite (Fig. 3). Smaller particle sizes reduce internal diffusion and mass transfer limitations to penetration of the adsorbate inside the adsorbent [31]. With unactivated attapulgite equilibrium is reached in 4 h to as opposed to 2 h for activated attapulgite. Since adsorption is pH dependent [32], activated attapulgite has more neutralizing cations (Na_2O, MgO and CaO) than unactivated attapulgite, hence adsorption is faster with activated attapulgite. The palygorskite structure of activated attapulgite (Fig. 2(d)) is almost collapsed, leading to a decrease in specific surface area. So reuse is limited, unlike unactivated attapulgite which has a higher specific surface area, allowing reuse. ΔS^0 values for unactivated attapulgite are higher than those of activated attapulgite, showing more affinity of unactivated attapulgite for metal ions than activated attapulgite [25], hence metals are immobilized more in unactivated attapulgite than in activated attapulgite. Q_{max} for Fe, Mn, Co, Cu and Ni for activated attapulgite are higher than those of unactivated attapulgite since an optimum solid loading of 2.5% was used for activated attapulgite as compared to 10% for unactivated attapulgite.

CONCLUSION

Activated attapulgite can be used to remove heavy metals and neutralize AMD at 2.5% m/v loading. The adsorption isotherms were better represented with the Langmuir isotherm. The process is exothermic for Fe and Ni and endothermic for Cu, Mn and Cu.

Fe, Cu, Ni and Fe adsorption was thermodynamically feasible while Mn adsorption is thermodynamically not feasible. Co adsorption becomes thermodynamically feasible at high temperatures. It was also noted that sulfate removal was poor with activated attapulgite. Metal-loaded activated attapulgite can be regenerated with 0.05 M HNO_3. Activation of attapulgite resulted in the reduction of adsorbent loading and residence time; however, it also resulted in poor immobilization of metal ions by activated attapulgite. It is recommended that a sulfate-binding ligand be incorporated on the surface of activated attapulgite to improve sulfate removal.

ACKNOWLEDGEMENT

REFERENCES

1. P. L. Younger, S. A. Banwart and R. S. Hedin, *Mine water hydrology, pollution, remediation*, Dordrecht, The Netherlands, Kluwer Academic (2002).
2. W. Stumm and J. J. Morgan, Aquatic Chemistry, 3rd Ed., Wiley, New York (1996).
3. Expert Team of the Inter-Ministerial Committee, *Mine water management in the Witwatersrand Gold Fields with special emphasis on acid mine drainage*, Report to the Inter-Ministerial Committee on Acid Mine Drainage. Pretoria: Department of Water Affairs (2010).

4. M. P. Filion, L. L. Siroois and K. Ferguson, *CIM Bulletin*, **83**, 33 (1990).

5. M. A. Caraballo, F. Macías, T. S. Rötting, J. M. Nieto and C. Ayora, *Environ. Pollut.*, **159**, 3613 (2011).

6. C. B. Murphy and S. J. Spiegel, *Water Pollut. Federat.*, **54**, 849 (1982).

7. C. A. Rios, C. D. Williams and C. L. Roberts, *J. Hazard. Mater.*, **156**, 23 (2008).

8. H. Zhang, Z. Tong, T. Wei and Y. Tang, *Desalination*, **276**, 103 (2011).

9. T. Falayi and F. Ntuli, *J. Ind. Eng. Chem.* (2013), http://dx.doi.org/10.1016/j.jiec.2013.07.007.

10. H. Tutu, T. S. McCarthy and E. Cukrowska, *Appl. Geochem.*, **23**, 3666 (2008).

11. R. L. Frost, C. A. Cash and J. T. Kloprogge, *Vibrational Spectroscopy*, **16**, 173 (1998).

12. J. Madejova and P. Komadel, *Clays Clay Min.*, **49**, 410 (2001).

13. W. Yan, D. Liu, D. Tan, P. Yuan and M. Chen, *Spectrochim. Acta Part A: Mol. Biomol. Spectroscopy*, **97**, 1052 (2012).

14. W. Hirsiger, M. Muller-Vonmoos and H. G. Wiedemann, *Thermochim. Acta*, **13**, 223 (1975).

15. G. E. Van-Scoyoc, C. J. Serna and J. L. Ahlrichs, *American Mineralogist*, **64**, 215 (1979).

16. J. B. Dixon and S. B. Weed, Minerals in Soil Environments, 2nd Ed. Soil Science Society of America, Wisconsin, USA (1989).

17. F. Ntuli and A. E. Lewis, *Chem. Eng. Sci.*, **64**, 2202 (2009).

18. F. Gan, J, Zhou, H. Wang, C. Du and X. Chen, *Water Res.*, **43**, 2907 (2009).

19. H. Ucum, Y. K. Baghan, Y. Kaya, A. Cakici and O. F. Algurb, *Desalination*, **154**, 233 (2003).

20. E. H. James, Inorganic Chemistry Principles, Harper & Row (1978).

21. R. S. Juang, F. C. Wu and R. L. Tseng, *Environ. Technol.*, **18**, 525 (1997).

22. R. E Tryball, Mass Transfers Operations, 3rd Ed., McGraw-Hill, New York (1980).

23. K. G. Bhattacharyya and S. S. Gupta, *Appl. Clay Sci.*, **41**, 1 (2008).

24. I. P. Okoye and C. Obi, *International Arch. Appl. Sci. Technol.*, **3**, 58 (2012).

25. V. K. Gupta, *Ind. Eng. Chem. Res.*, **37**, 192 (1998).

26. M. G. A. Vieira, A. F. Almeida Neto, M. L. Gimenes and M. G. C. da Silva, *J. Hazard. Mater.*, **177**, 362 (2010).

27. M. Balintova, M. Holub and E. Singovszka, *Chem. Eng. Trans.*, **28**, 1 (2012).

28. B. Boonchom, S. Youngme, S. Maensiri and C. Danvirutai, *J. Alloys Compd.*, **454**, 78 (2008).

29. X. D. Liu, M. Hagihala, X. G. Zheng, D. D. Meng and D. X. Guo, *Chinese Physics Letters*, **28**, 1 (2011).

30. L. Paavo and T. Jouni, *ActaChemicaScandinavica*, **27**, 2287 (1973).

31. A, Mohammad, *Desalination*, **250**, 885 (2010).

32. G. Sposito, *The Chemistry of Soils*, New York, Oxford University Press (1989).